PHYSICS

Fast topological pumps via quantum metric engineering on photonic chips

Wange Song[1]†, Oubo You[2]†, Jiacheng Sun[1], Shengjie Wu[1], Chen Chen[1], Chunyu Huang[1], Kai Qiu[1], Shining Zhu[1], Shuang Zhang[2,3,4]*, Tao Li[1]*

Topological pumps have garnered substantial attention in physics. However, the requirement for slow evolution speed to satisfy adiabaticity greatly restricts their application in on-chip devices. Here, we discover a direct link between adiabaticity and quantum metric, the real part of quantum geometry that has been relatively less explored compared to its imaginary counterpart, the Berry curvature. We demonstrate that the evolution speed of topological pumps between nontrivial edge states can be increased by reducing the quantum metric via introduction of long-range coupling to the celebrated Rice-Mele model. This fast topological pump can occur without affecting the bulk state evolution, which challenges the common understanding. We experimentally confirm our findings by using a platform consisting of bilayer integrated silicon waveguides operating at telecommunication wavelengths. Our work provides possibilities for lifting topological pumps from the constraints of slow evolution and paves the way toward compact photonic integration.

INTRODUCTION

In physics, topology could emerge from the slow cyclic variation of parameters that satisfies the adiabatic condition (*1*–*3*). The Thouless pump, which shares the same topological origin as the quantum Hall effect, serves as an important manifestation of topological physics (*4*–*12*). It describes the quantized transfer of particles per cycle of evolution in the parameter space and remains robust against deformation of the evolution loop in the adiabatic regime. While initially proposed in solid-state electronic systems, the Thouless pump has been observed in diverse systems, including ultracold atoms (*13*–*15*), mechanics (*16*), acoustics (*17*–*21*), and photonic waveguides (*22*–*34*). Thouless pumps in d spatial dimensions manifest states that cross the energy gap and localize on their $(d-1)$–dimensional boundaries (*16*, *22*, *27*, *35*). The adiabatic evolution of these states has been exploited to realize robust transport of energy from one edge of a finite system to the opposite one (*16*, *22*, *24*, *27*, *31*, *32*, *34*, *35*). This effect is connected to the appearance, in the Hamiltonian spectrum, of gapless points enclosed by the adiabatic loop in the parameter space. In photonics, it manifests as the transfer of localized light field from one end to another, which may have potential applications in optical routing (*22*, *24*, *32*, *33*) and quantum information processing (*36*–*38*).

Similar to many other topological effects, adiabaticity plays an essential role in achieving topological pumps. Deviation from adiabaticity will inevitably cause undesired states to be populated and eventually result in breakdown of the pump (*10*). Despite its fundamental importance, adiabaticity itself and its engineering in topological pumps remain largely unexplored. The most common way to achieve adiabaticity is to slow down the evolution of the system. However, this increases the evolution duration of the system and reduces the compactness of most waveguide systems, limiting the potential utilization of topological devices. Thus, there is an urgent need to find a solution to manipulate and relax the adiabatic criteria in topological pumps.

Adiabaticity describes the ability of the system to maintain the population of the instantaneous eigenstates during evolution. The adiabaticity criterion is usually defined by $\hbar|\langle\psi_m|\partial_t|\psi_n\rangle/(\varepsilon_m-\varepsilon_n)|\ll 1$ (*39*–*42*), which involves not only the instantaneous eigenstates (i.e., the numerator) but also their energy difference (the denominator). However, it only describes the transition amplitude between a pair of eigenstates. If the system consists of multiple eigenstates, it is not very straightforward to evaluate the adiabaticity condition for the evolution of a particular populated eigenstate due to the presence of multiple transition paths to all other eigenstates. Here, we propose a criterion to describe the adiabaticity of a populated eigenstate, namely, the quantum metric $|\det(g)|$, with g being the quantum metric tensor (QMT), which is the real part of the quantum geometry defining the distance between two neighboring eigenstates in the projected Hilbert space (*43*–*51*) (see also text S2 for more details). We discover a negative correlation between the quantum metric and the adiabaticity condition. Specifically, a smaller quantum metric results in improved adiabaticity for the system. As an example, we show that introducing next-nearest-neighboring (NNN) couplings into the Rice-Mele (RM) model (*52*) can reduce the quantum metric of the pumping channel and promise a fast evolution speed. More interestingly, we find that the bulk state evolution is exactly the same with or without this NNN coupling, reflecting that topological pump is not determined solely by bulk state property, in contrast to common notion. For the experimental implementation, we propose and fabricate a bilayer integrated silicon waveguide lattice with controllable inter- and intra-layer couplings, which enables effective long-range interaction in the system. On the basis of this platform, we demonstrate a topological boundary pump in a highly compact optical system, which would not be expected in a system with only nearest-neighbor (NN) coupling under rapid parameter evolution. Moreover, in contrast to the single-layer architecture of most photonic integrated circuits demonstrated so far, our work develops a

[1]National Laboratory of Solid State Microstructures, Key Laboratory of Intelligent Optical Sensing and Manipulations, Jiangsu Key Laboratory of Artificial Functional Materials, College of Engineering and Applied Sciences, Nanjing University, Nanjing 210093, China. [2]New Cornerstone Science Laboratory, Department of Physics, University of Hong Kong, Hong Kong, China. [3]Department of Electronic and Electrical Engineering, University of Hong Kong, Hong Kong, China. [4]Materials Innovation Institute for Life Sciences and Energy (MILES), HKU-SIRI, Shenzhen, P.R. China.
*Corresponding author. Email: shuzhang@hku.hk (S.Z.); taoli@nju.edu.cn (T.L.)
†These authors contributed equally to this work.

layered integrated silicon platform and demonstrates the ability to achieve robust light transfer between layers, thereby expanding on-chip photonic integration from two-dimensional (2D) to quasi-2D and even to 3D. This advancement enables improved integration of photonic chips and provides a dimension for achieving more sophisticated on-chip photonic manipulations at the nanoscale.

RESULTS

Relation between adiabaticity and quantum metric

For a quantum system populated by only a single eigenstate, the adiabaticity can be measured by how much it deviates from this instantaneous eigenstate after a short time interval δt. Considering such a time-dependent system with Hamiltonian $H(t)$, the infinitesimal time evolution operator $U(t_0+\delta t, t_0) = \exp\left[-i/\hbar \int_{t_0}^{t_0+\delta t} H(t')dt'\right]$ can be expanded with respect to δt up to the second order

$$U(t_0+\delta t, t_0) = 1 - \frac{i}{\hbar}H(t_0)\delta t + \frac{1}{2}\left\{\left[-\frac{i}{\hbar}H(t_0)\right]^2 + \left[-\frac{i}{\hbar}H'(t_0)\right]\right\}\delta t^2 \quad (1)$$

where $H'(t)$ is the derivative with respect to time. In a similar way, the instantaneous eigenstate $|\psi_n(t+\delta t)\rangle$ can also be expanded

$$|\psi_n(t_0+\delta t)\rangle = |\psi_n(t_0)\rangle + |\psi_n'(t_0)\rangle\delta t + \frac{|\psi_n''(t_0)\rangle}{2}\delta t^2 \quad (2)$$

The adiabaticity condition can thus be characterized by $|\langle\psi_n(t_0+\delta t)|U(t_0+\delta t, t_0)|\psi_n(t_0)\rangle|^2$, which represents how much of the initial populated eigenstate would remain on the same eigenstate after a short evolution time δt, and is related to the quantum metric by the following expression (see text S3 for details):

$$\frac{1-|\langle\psi_n(t_0+\delta t)|U(t_0+\delta t, t_0)|\psi_n(t_0)\rangle|^2}{\delta t^2} = |g| + O(\delta t) \quad (3)$$

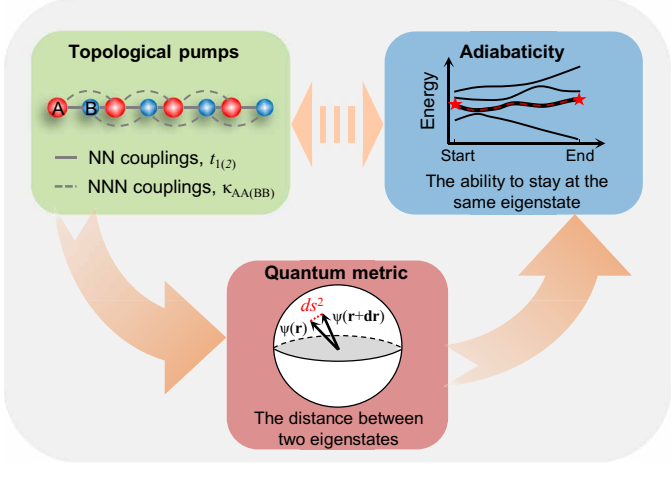

Fig. 1. Illustration of connections between the topological pumps, adiabaticity, and quantum metric. The quantum metric establishes an elegant way to quantitatively evaluate the adiabaticity and explain the pumping behaviors, especially when multiple parameters (e.g., involving the NNN couplings) interact together.

where $|g| = |\langle\psi'_n|\psi'_n\rangle - \langle\psi'_n|\psi_n\rangle\langle\psi_n|\psi'_n\rangle|$ is the quantum metric (*43*–*51*). This expression shows that adiabaticity is directly linked to the quantum metric. In contrast to the commonly adopted adiabaticity criterion that involves at least a pair of eigenstates (*39*–*42*), this criterion uses the information of only the populated eigenstate, thus can be termed instantaneous self-adiabaticity (ISA). The ISA contains all the transitions between the populated eigenstate and others; thus, it is more convenient and efficient compared to the conventional adiabaticity criterion (see text S4 for details). Our expression (Eq. 3) shows that by reducing the quantum metric in the system, the adiabatic condition can be better satisfied. As such, the evolution process can be sped up while maintaining the adiabaticity. In the following sections, we illustrate our idea by a specific case, i.e., fast topological pumps in an RM setup with long-range coupling, in which the NNN coupling affects the adiabaticity via quantum metric engineering (see schematics in Fig. 1).

Influence of long-range couplings on the quantum metric

The tight-binding Hamiltonian of an NNN coupling–modified RM model writes

$$H(\phi) = H_{\text{onsite}}(\phi) + H_{\text{NN}}(\phi) + H_{\text{NNN}}(\phi) \quad (4)$$

where ϕ is the pump parameter corresponding to the synthetic momentum, and H_{onsite}, H_{NN}, and H_{NNN} represent the on-site energy, NN coupling, and NNN coupling terms, respectively

$$\begin{aligned} H_{\text{onsite}}(\phi) &= \sum_{j=1}^{N}\left[\beta_A(\phi)\hat{a}^\dagger_{A,j}\hat{a}_{A,j} + \beta_B(\phi)\hat{a}^\dagger_{B,j}\hat{a}_{B,j}\right] \\ H_{\text{NN}}(\phi) &= \sum_{j=1}^{N}\left[t_1(\phi)\hat{a}^\dagger_{B,j}\hat{a}_{A,j} + t_2(\phi)\hat{a}^\dagger_{A,j+1}\hat{a}_{B,j} + h.c.\right] \\ H_{\text{NNN}}(\phi) &= \sum_{j=1}^{N-1}\left[\kappa_{AA}(\phi)\hat{a}^\dagger_{A,j+1}\hat{a}_{A,j} + \kappa_{BB}(\phi)\hat{a}^\dagger_{B,j+1}\hat{a}_{B,j} + h.c.\right] \end{aligned} \quad (5)$$

where N is the total number of unit cells. $\beta_A(\phi)$ and $\beta_B(\phi)$ are staggered on-site potentials, $t_1(\phi)$ and $t_2(\phi)$ are the NN couplings, and $\kappa_{AA}(\phi)$ and $\kappa_{BB}(\phi)$ are the NNN couplings, which are all ϕ-dependent. Specifically, we consider sinusoidal modulations (see Fig. 2B), with β_0, t_0, and κ_0 being the averaged quantities, and β', t', and κ' being the corresponding modulation strength. We define $\Delta\beta \equiv \beta_B - \beta_A$, $\Delta\kappa \equiv \kappa_{BB} - \kappa_{AA}$, and $\Delta t \equiv t_2 - t_1$. In the thermodynamic limit (N large), the Hamiltonian shows two energy bands (valence and conduction bands) separated by a gap of width $\Delta\varepsilon = 2\sqrt{(\Delta\beta/2-\Delta\kappa)^2 + (\Delta t)^2}$. It can be proven that the topological pump property is determined by the parameter evolution trajectory in the 2D $(\Delta\beta/2 - \Delta\kappa, \Delta t)$ parameter space (see text S1). As shown in Fig. 2A, the trajectory of the adiabatic pump encircles the critical gap-closing point $(\Delta\beta/2 - \Delta\kappa = \Delta t = 0)$ in the $(\Delta\beta/2 - \Delta\kappa, \Delta t)$ parameter space, and thus indicates a nontrivial topological pump.

Figure 2C illustrates such a process by showing the Wannier centers (WCs) (*27*, *34*, *53*, *54*) of the pumping cycle (red dashed curves). The cycle transports a WC across one unit cell, which is equivalent to the quantization of particle transport, i.e., the Chern number. Note that our case reduces to a conventional RM setting of topological pump if there are no H_{NNN} terms [i.e., $\kappa_{AA}(z) = \kappa_{BB}(z) \equiv 0$] (*30*–*32*). The WC evolution for conventional RM pump is also shown as the reference (black dashed curves in Fig. 2C). They demonstrate exactly the same evolution path and quantization (Chern # = 1)

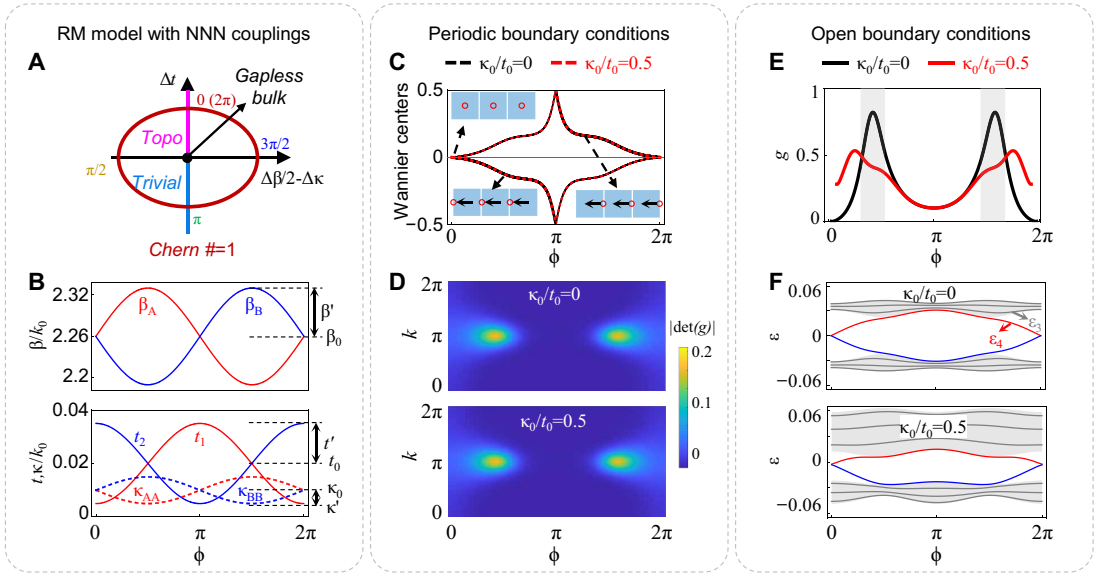

Fig. 2. Quantum metric in the RM model with NNN couplings. (**A**) Trajectory of pump cycle in the 2D parameter space ($\Delta\beta/2 - \Delta\kappa$, Δt). (**B**) The ϕ-dependent on-site potentials (β_A and β_B), NN couplings (t_1 and t_2), and NNN couplings (κ_{AA} and κ_{BB}). (**C**) Evolutions of Wannier center (WC) of the bands during a pump cycle. Black dashed curve for traditional RM pump with $\kappa_0/t_0 = 0$ and red dashed curve for $\kappa_0/t_0 = 0.5$. During a cycle, each WC of the valence (thick) and conduction (thin) band moves to the left and right with a single lattice constant. Inset: schematic of the evolution of the WC (hollow circles) during one cycle of a topological pump. (**D**) The quantum metric $|\det(g)|$ in the momentum space k and parameter space ϕ for $\kappa_0/t_0 = 0$ (top) and 0.5 (bottom) under periodic boundary conditions. (**E**) Quantum metric distribution along the pumping parameter ϕ for $\kappa_0/t_0 = 0$ and 0.5 under open boundary conditions. (**F**) Energy spectra as a function of ϕ for $\kappa_0/t_0 = 0$ and $\kappa_0/t_0 = 0.5$. The red and blue curves are the pump channels. The light-gray background represents the bulk region and dark-gray curves are the bulk bands.

for a complete pump cycle (red and black dashed curves). The bulk state evolution relies on the how eigenstate is distributed in parameter space or, more mathematically speaking, how the eigenstate fiber bundle lives on the parameter base manifold; there is a natural geometric structure of this fiber bundle called quantum geometric tensor (QGT) (*43*). The well-known Berry curvature actually defines the imaginary part of the QGT (crucial for topological matter), and its real part is referred to as the QMT, reflecting the distance between two neighboring eigenstates in the parameter space (*43*–*51*). The same fiber bundle structure leads to the same QGT, that is, the same Berry curvature (i.e., the same WC evolution, see Fig. 2C) and quantum metric (Fig. 2D; see text S2 for details) with or without the NNN couplings, implying that their bulk state evolutions are the same [here, the bulk mode evolutions are the evolving of Bloch mode in the (ϕ, k) spaces]. This is because the NNN hoppings only change the eigenenergy but do not affect the eigenstate of the Bloch mode (see text S1). Note that all the above results are obtained based on the periodic boundary condition. The quantum metric can be influenced by the NNN coupling if a finite system with topological edge states is considered, as will be shown below.

Note that, at $\phi = 0$, one has $\Delta\beta = \Delta\kappa = 0$ and $\Delta t > 0$, which indicates the nontrivial topological phase (indicated by the pink line in Fig. 2A) and thus supports two zero-energy instantaneous topological states located at the two edge sites (either left or right) for a finite chain with open boundaries. Figure 2F shows the band structure of a finite system ($2N = 8$) with respect to the pump parameter ϕ for a typical open boundary with $\kappa_0/t_0 = 0$ and $\kappa_0/t_0 = 0.5$, respectively, where the red and blue solid curves represent the pump channels inside the bulk bandgap. Starting at $\phi = 0$ with one of the two eigenstates (e.g., with eigenstate localized at the left edge) and adiabatically evolving such an eigenstate along the top pump channel (red curve), this state is transformed into the right-edge state after one cycle, i.e., at $\phi = 2\pi$, thus realizing the edge-to-edge topological pumps. Notably, the topological pumping process requires adiabatic conditions; i.e., the excitations should remain at the pump channel even if the system is varied (*39*–*42*). Figure 2E illustrates the distribution of the quantum metric $g = \delta s^2/\delta\phi^2$ under open boundary conditions for the pumping channel (left-to-right pumping channel) along the ϕ with $\kappa_0/t_0 = 0$ and $\kappa_0/t_0 = 0.5$, respectively [here, δs^2 is the quantum distance between $\psi(\phi)$ and $\psi(\phi + \delta\phi)$ in the pumping parameter space]. Two peaks of g emerge at $\phi \sim \pi/2$ and $3\pi/2$ for the traditional topological pumping process (black curve in Fig. 2E). The inclusion of the NNN coupling leads to a noticeable suppression of the peaks of the quantum metric (red curve in Fig. 2E), thus relaxing the adiabatic condition and giving rise to a faster evolution.

Illustration of quantum metric empowered fast topological pumps

To quantitatively assess the adiabaticity of the pumping process, we consider an optical waveguide model and introduce the quantity $\eta(\phi) \equiv |\langle\psi(\phi)|\Phi(\phi)\rangle|^2$, where $\psi(\phi)$ is the instantaneous eigenstate on the pumping channel and $\Phi(\phi)$ denotes the actual distribution of light field at ϕ. Notably, $\eta(\phi = 2\pi)$ serves as a measure of the fidelity of the entire pumping process. We numerically compute the fidelity $\eta(2\pi)$ as a function of the pump speed (ω) for $\kappa_0/t_0 = 0$ (black curve) and 0.5 (red curve), respectively (see Fig. 3A). The η can be maintained close to 1 for a slow varying speed (the adiabaticity is satisfied). However, as the speed exceeds a critical value ω_c, the curves exhibit oscillating features (indicating

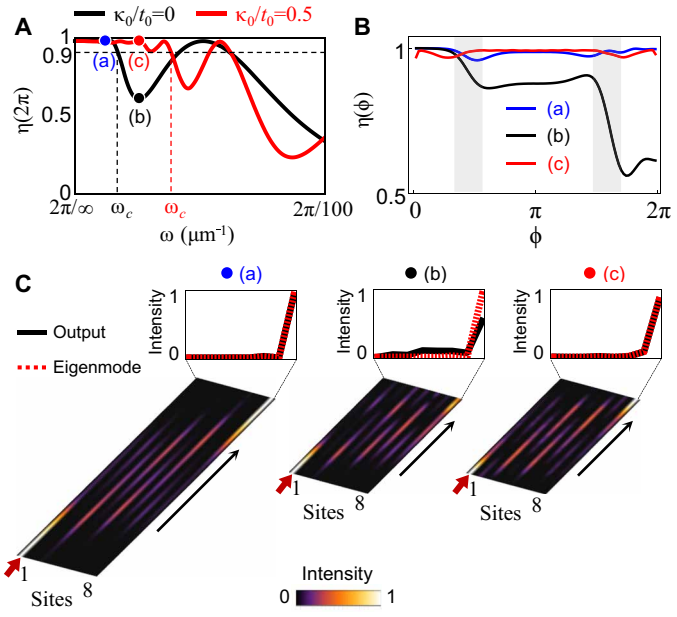

Fig. 3. Illustration of quantum metric empowered fast topological pumps. (**A**) Fidelity of topological pumps as a function of the pump speed for $\kappa_0/t_0 = 0$ and 0.5. (**B**) Fidelity of the eigenmodes on the pump channel for the pump evolutions shown in (C). (**C**) Light evolutions of topological pumps corresponding to the cases marked in (A).

nonadiabaticity). According to Fig. 3A, the critical speed ω_c is $2\pi/690\ \mu m^{-1}$ (for $\eta > 0.9$) for the traditional topological pump ($\kappa_0/t_0 = 0$) and can be increased to $2\pi/314\ \mu m^{-1}$ for $\kappa_0/t_0 = 0.5$ (note that the critical speed ω_c can be estimated according to their quantum metrics, see text S5). This suggests the possibility of achieving a twofold speed-up in the topological pump. To illustrate this, we analyze the topological pump in three cases with different κ_0/t_0 values and pump speeds, marked by the blue, black, and red dots in Fig. 3A. The fidelity of the edge mode along the evolution $\eta(\phi)$ and the corresponding optical field evolutions are illustrated in Fig. 3 (B and C, respectively). For conventional topological pump ($\kappa_0/t_0 = 0$) with low pump speed ($\omega = 2\pi/900\ \mu m^{-1}$, blue dot), the optical field injected from one edge transports to the other edge after each pump cycle [see Fig. 3C (a)]. $\eta(\phi)$ remains consistently close to unity throughout the evolution (Fig. 3B, blue curve), confirming the fulfillment of the adiabatic condition. However, if the pump speed is increased, for example, to $\omega = 2\pi/475\ \mu m^{-1}$, the adiabatic condition is broken, leading to transitions to undesired states during the evolution [Fig. 3B, black curve, $\eta(\phi)$ decreases to ~0.5]. In such a scenario, the pump for the original RM model would fail and the optical field would couple to the bulk states [see Fig. 3C (b)]. In contrast, for the same fast pump speed but with $\kappa_0/t_0 = 0.5$ [as shown in Fig. 3C (c)], nearly all the input from the left side can be transferred to the other side and $\eta(\phi)$ maintains close to unity throughout evolutions (Fig. 3B, red curve), confirming the retrieval of adiabatic topological pumps. Note the fidelity η is related to the quantum metric g. A large g indicates a high transition probability between eigenstates, so the populated eigenstate tends not to stay on its energy level and thus decreases the fidelity. As shown in Fig. 3B, the fidelity η drops rapidly in the vicinity of $\phi \sim \pi/2$ and $3\pi/2$ (black curve, gray region), where exactly the peaks of quantum metric g appear (Fig. 2E). These light propagation results are consistent with the prediction from the quantum metric, indicating that these effects can possibly be observed in experiments.

Experimental observations in waveguides

We implement our model on an integrated photonic waveguide platform (*55*–*64*) with periodically modulated propagation constant, inter- and intra-layer couplings along the z direction (serves as synthetic time t). It comprises eight silicon waveguides arranged into two layers, featuring a distinctive zigzag configuration as depicted in Fig. 4 (A and B). The bottom layer is placed on the sapphire substrate and surrounded by SU-8, and the top layer is also embedded in SU-8. The pumping parameter $\phi \equiv \omega z$, where ω represents the pump speed (i.e., modulation frequency, $\omega \equiv 2\pi/L$, where L is the total waveguide length). The propagation constants and coupling coefficients are carefully designed according to the principles outlined in text S7, ensuring that they meet the requirements of the model. In experiments, we fabricate bilayer-integrated waveguide samples (see SEM pictures in Fig. 4, D and E), as well as a conventional single-layer sample (Fig. 4F) for comparison (see Materials and Methods for sample fabrications). All the waveguides are fanned out and connected to the grating couplers for light input ($I_1 \ldots I_8$) and output ($O_1 \ldots O_8$) (see Fig. 4C).

We first demonstrate the conventional topological pump based on the integrated waveguide array. Figure 5A (bottom) shows the full-wave simulation of optical field evolutions for the single-layer sample ($\kappa_0/t_0 = 0$). The light (1550 nm) injected into waveguide 1 is lastly transported to waveguide 8, demonstrating the topological pump process. Note that the length of the system (~600 μm) is quite long to satisfy the adiabatic condition. When the length is shortened to 250 μm, the optical field sinks into the bulk and the pump fails (see Fig. 5B, bottom). Conversely, for a bilayer waveguide architecture with effective NNN coupling ($\kappa_0/t_0 = 0.5$, with all other parameters being kept the same as those in the single-layer waveguides for a fair comparison), the formerly nonadiabatic process can be turned into adiabatic due to the suppressed quantum metric, and thereby the topological pump persists even at a short length of 250 μm. This is shown in Fig. 5C (bottom), where the light input from waveguide 1 of the bottom layer is transported to waveguide 8 of the top layer. In experiments, a 1550-nm laser beam is input from port I_1, and the output signal can be directly observed from the scattering by the output grating couplers ($O_1, \ldots, O_8$) (see Fig. 5, middle panels). The experimental results agree well with the simulation (see Fig. 5, top panels)—the fabricated bilayer samples can successfully pump the signal to the other side, while the pump fails for the conventional single-layer configuration when the length is relatively short. Note that the fast pump process here is indeed in adiabatic condition; i.e., further increasing the length of the bilayer structure would yield a similar pump effect (see text S8 for details). In addition, the evolution length can be further reduced to an extremely short length of 34 μm considering a nonadiabatic process, about $^1/_{20}$ the length of the conventional topological pump (see text S9). In this case, the edge state is allowed to couple to the bulk states and then back to the pump channel to achieve light transfer to the other side, which opens possibilities in chip-scale photonics manipulations.

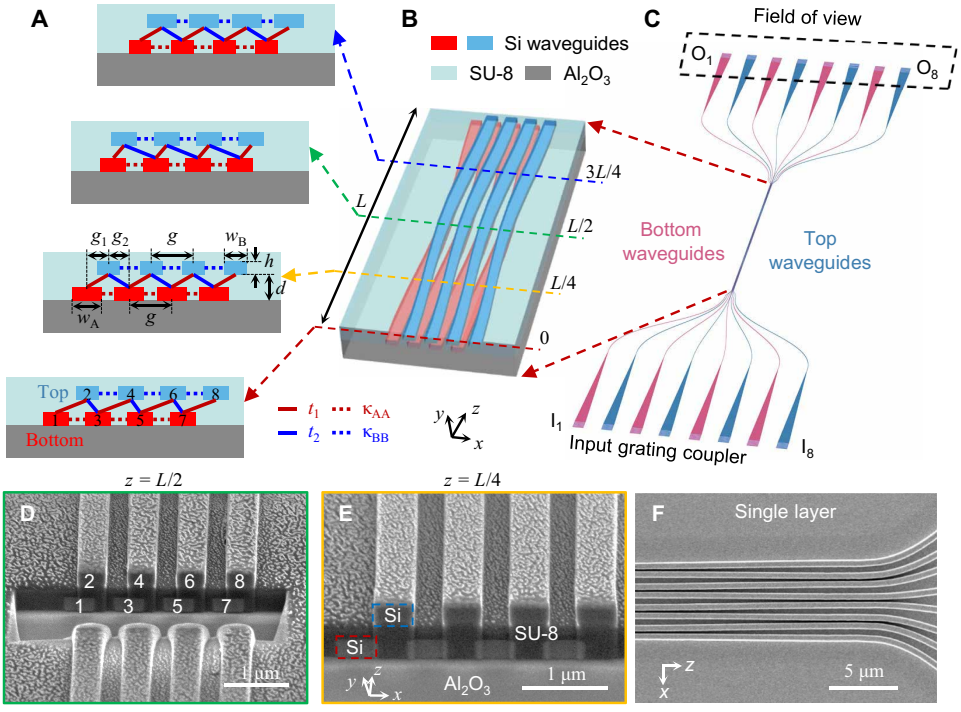

Fig. 4. Design of bilayer integrated silicon waveguides. Cross section for different pumping stages (**A**) and full view (**B**) of the bilayer waveguide systems. (**C**) Schematics of experimental sample design. Scanning electron microscope (SEM) images at different locations of the same bilayer sample, showing waveguides' cross section at $z = L/2$ (**D**) and $z = L/4$ (**E**). Note the images are captured before coating the top SU-8 film. The focused ion beam (FIB) is used to dig holes on the surface of the sample to expose the bottom waveguides. (**F**) SEM image of a single-layer sample.

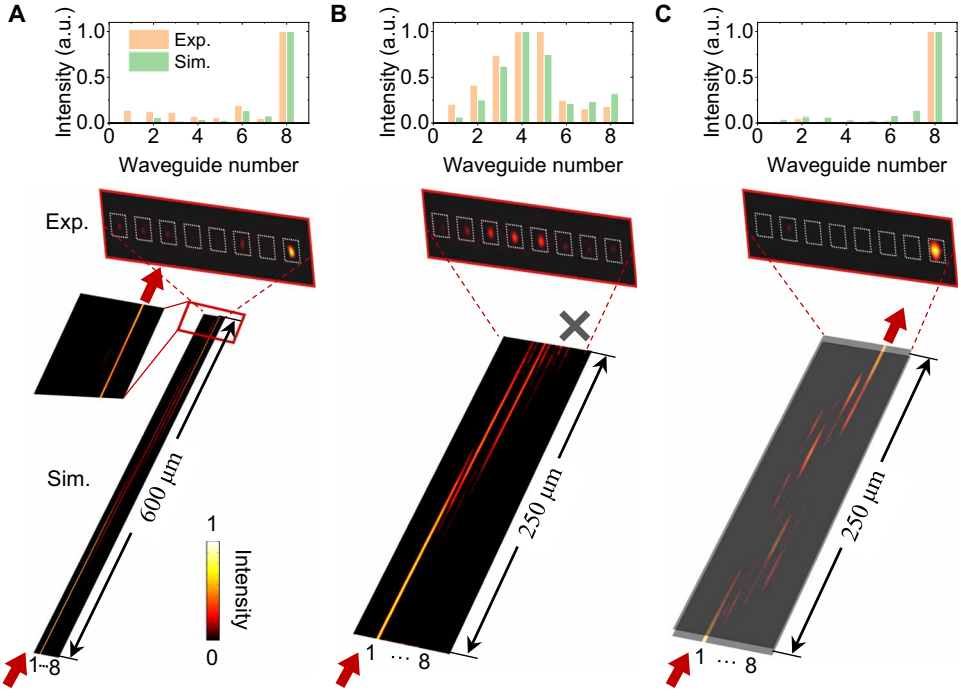

Fig. 5. Experimental observation of fast topological pumps. Simulated light propagations (bottom), experimentally captured intensities (middle) at the output facet, and optical intensity profiles (top) of simulations (green bars) and experiments (orange bars) for the single-layer samples with 600-μm (**A**) and 250-μm (**B**) length, and for bilayer samples with 250-μm (**C**) length.

DISCUSSION

It should be noted that although the fast topological pump behaviors may also be intuitively understood from the perspective of adiabatic elimination (*65*) or direct NNN coupling picture, they fail to capture the adiabaticity of the pumping process (see text S6). Moreover, the distribution of the quantum metric can capture all the distinct peaks in all conventional criteria's distributions (see text S4 for details). Therefore, the quantum metric establishes an elegant way to quantitatively evaluate the adiabaticity and explain the pumping behaviors. It has been commonly believed that the topological pump of nontrivial edge state in a finite system with open boundary is solely determined by the corresponding bulk state evolution. However, our work uncovers an intriguing phenomenon that the topological pump of edge states can differ between systems sharing exactly the same bulk state evolution. Specifically, the bilayer pumps show more relaxed adiabaticity, are more robust against nonadiabaticity arising from the fast parameter evolution, and thus give rise to fast topological pumps compared to the conventional case.

In summary, our research demonstrated the equivalence between instantaneous self-adiabaticity and the quantum metric, which would be as important as Berry curvature but less explored. This criterion is more convenient for inspecting the adiabaticity of one eigenstate populated question without sacrificing any critical information. As an example, we introduce NNN hopping into the celebrated RM model. Although the bulk state evolution remains unchanged, the quantum metric associated with the pump channel decreases, which contrasts with common sense. This decreased quantum metric leads to the achievement of a fast topological pump with half the evolution length compared to the case without NNN hopping. This breakthrough paves the way toward compact integrated devices that are compatible with current integrated photonic fabrication techniques. Furthermore, our bilayer integrated platform with tunable interlayer couplings provides more degrees of freedom in integrated photonic designs, which can potentially lead to the development of more efficient and versatile photonic devices.

MATERIALS AND METHODS

The waveguides and grating nanostructures are fabricated using the method of electron beam lithography and inductively coupled plasma (ICP) etching process. The substrate used herein is 220-nm silicon deposition on a 460-μm alumina substrate, and the substrates are cleaned in ultrasound bath in acetone and deionized water for 10 min, and dried under clean nitrogen flow. Then, a layer of MA-N2405 photoresist film is spin-coated onto the substrate and baked at 90°C for 3 min. After that, the sample is exposed to electron beam in an E-beam writer (Elionix, ELS-F125) and developed to form the MA-N2405 nanostructures. Then, the sample is transferred into an HSE Series Plasma Etcher 200 and etched with C_4F_8 and SF_6 (the flow rates of these two types of gases are 75 and 30 standard cubic centimeters per minute). After the ICP etching, the remaining MA-N2405 is removed by using an O_2 plasma for 5 min. Before the fabrication of the second layer of nanostructures, a 530-nm SU-8 resist is spin-coated onto the sample and baked at 200°C for 30 min. Then, another α-Si layer was deposited on the SU-8 using the plasma-enhanced chemical vapor deposition to a final thickness of 220 nm. Repeat the process of the first layer structure afterward to form the top layer nanostructure. Last, another SU-8 is spin-coated onto the sample for protection (see fig. S8 for the fabrication flow).

Supplementary Materials

This PDF file includes:

Text S1 to S9
Figs. S1 to S10
References

REFERENCES AND NOTES

1. L. Lu, J. D. Joannopoulos, M. Soljacic, Topological photonics. *Nat. Photon.* **8**, 821–829 (2014).
2. T. Ozawa, H. M. Price, A. Amo, N. Goldman, M. Hafezi, L. Lu, M. C. Rechtsman, D. Schuster, J. Simon, O. Zilberberg, I. Carusotto, Topological photonics. *Rev. Mod. Phys.* **91**, 015006 (2019).
3. M. Kim, Z. Jacob, J. Rho, Recent advances in 2D, 3D and higher-order topological photonics. *Light Sci. Appl.* **9**, 130 (2020).
4. D. J. Thouless, Quantization of particle transport. *Phys. Rev. B* **27**, 6083–6087 (1983).
5. Q. Niu, D. J. Thouless, Quantised adiabatic charge transport in the presence of substrate disorder and many-body interaction. *J. Phys. A* **17**, 2453–2462 (1984).
6. L. Wang, M. Troyer, X. Dai, Topological charge pumping in a one-dimensional optical lattice. *Phys. Rev. Lett.* **111**, 026802 (2013).
7. L. Taddia, E. Cornfeld, D. Rossini, L. Mazza, E. Sela, R. Fazio, Topological fractional pumping with alkaline-earth-like atoms in synthetic lattices. *Phys. Rev. Lett.* **118**, 230402 (2017).
8. W. Ma, L. Zhou, Q. Zhang, M. Li, C. Cheng, J. Geng, X. Rong, F. Shi, J. Gong, J. Du, Experimental observation of a generalized Thouless pump with a single spin. *Phys. Rev. Lett.* **120**, 120501 (2018).
9. M. H. Kolodrubetz, F. Nathan, S. Gazit, T. Morimoto, J. E. Moore, Topological Floquet-Thouless energy pump. *Phys. Rev. Lett.* **120**, 150601 (2018).
10. L. Privitera, A. Russomanno, R. Citro, G. E. Santoro, Nonadiabatic breaking of topological pumping. *Phys. Rev. Lett.* **120**, 106601 (2018).
11. Q. Fu, P. Wang, Y. V. Kartashov, V. V. Konotop, F. Ye, Two-dimensional nonlinear Thouless pumping of matter waves. *Phys. Rev. Lett.* **129**, 183901 (2022).
12. R. Citro, M. Aidelsburger, Thouless pumping and topology. *Nat. Rev. Phys.* **5**, 87–101 (2023).
13. S. Nakajima, T. Tomita, S. Taie, T. Ichinose, H. Ozawa, L. Wang, M. Troyer, Y. Takahashi, Topological Thouless pumping of ultracold fermions. *Nat. Phys.* **12**, 296–300 (2016).
14. M. Lohse, C. Schweizer, O. Zilberberg, M. Aidelsburger, I. Bloch, A Thouless quantum pump with ultracold bosonic atoms in an optical superlattice. *Nat. Phys.* **12**, 350–354 (2016).
15. M. Lohse, C. Schweizer, H. M. Price, O. Zilberberg, I. Bloch, Exploring 4D quantum Hall physics with a 2D topological charge pump. *Nature* **553**, 55–58 (2018).
16. I. H. Grinberg, M. Lin, C. Harris, W. A. Benalcazar, C. W. Peterson, T. L. Hughes, G. Bahl, Robust temporal pumping in a magneto-mechanical topological insulator. *Nat. Commun.* **11**, 974 (2020).
17. W. Cheng, E. Prodan, C. Prodan, Experimental demonstration of dynamic topological pumping across incommensurate bilayered acoustic metamaterials. *Phys. Rev. Lett.* **125**, 224301 (2020).
18. H. Chen, H. Zhang, Q. Wu, Y. Huang, H. Nguyen, E. Prodan, X. Zhou, G. Huang, Creating synthetic spaces for higher-order topological sound transport. *Nat. Commun.* **12**, 5028 (2021).
19. Z.-G. Chen, W. Tang, R.-Y. Zhang, Z. Chen, G. Ma, Landau-Zener transition in the dynamic transfer of acoustic topological states. *Phys. Rev. Lett.* **126**, 054301 (2021).
20. L.-S. Zeng, Y.-X. Shen, Y.-G. Peng, D.-G. Zhao, X.-F. Zhu, Selective topological pumping for robust, efficient, and asymmetric sound energy transfer in a dynamically coupled cavity chain. *Phys. Rev. Appl.* **15**, 064018 (2021).
21. O. You, S. Liang, B. Xie, W. Gao, W. Ye, J. Zhu, S. Zhang, Observation of non-Abelian Thouless pump. *Phys. Rev. Lett.* **128**, 244302 (2022).
22. Y. E. Kraus, Y. Lahini, Z. Ringel, M. Verbin, O. Zilberberg, Topological states and adiabatic pumping in quasicrystals. *Phys. Rev. Lett.* **109**, 106402 (2012).
23. Y. Ke, X. Qin, F. Mei, H. Zhong, Y. S. Kivshar, C. Lee, Topological phase transitions and Thouless pumping of light in photonic waveguide arrays. *Laser Photon. Rev.* **10**, 995–1001 (2016).
24. O. Zilberberg, S. Huang, J. Guglielmon, M. Wang, K. P. Chen, Y. E. Kraus, M. C. Rechtsman, Photonic topological boundary pumping as a probe of 4D quantum Hall physics. *Nature* **553**, 59–62 (2018).
25. A. Cerjan, M. Wang, S. Huang, K. P. Chen, M. C. Rechtsman, Thouless pumping in disordered photonic systems. *Light Sci. Appl.* **9**, 178 (2020).
26. M. Jürgensen, S. Mukherjee, M. C. Rechtsman, Quantized nonlinear Thouless pumping. *Nature* **596**, 63–67 (2021).
27. W. A. Benalcazar, J. Noh, M. Wang, S. Huang, K. P. Chen, M. C. Rechtsman, Higher-order topological pumping and its observation in photonic lattices. *Phys. Rev. B* **105**, 195129 (2022).

28. M. Jürgensen, S. Mukherjee, C. Jörg, M. C. Rechtsman, Quantized fractional Thouless pumping of solitons. *Nat. Phys.* **19**, 420–426 (2023).
29. P. Wang, Q. Fu, R. Peng, Y. V. Kartashov, L. Torner, V. V. Konotop, F. Ye, Two-dimensional Thouless pumping of light in photonic moiré lattices. *Nat. Commun.* **13**, 6738 (2022).
30. Z. Fedorova, H. Qiu, S. Linden, J. Kroha, Observation of topological transport quantization by dissipation in fast Thouless pumps. *Nat. Commun.* **11**, 3758 (2020).
31. Q. Cheng, H. Wang, Y. Ke, T. Chen, Y. Yu, Y. S. Kivshar, C. Lee, Y. Pan, Asymmetric topological pumping in nonparaxial photonics. *Nat. Commun.* **13**, 249 (2022).
32. L. Sun, H. Wang, Y. He, Y. Zhang, G. Tang, X. He, J. Dong, Y. Su, Broadband and fabrication tolerant power coupling and mode-order conversion using Thouless pumping mechanism. *Laser Photon. Rev.* **16**, 2200354 (2022).
33. Y.-K. Sun, X.-L. Zhang, F. Yu, Z.-N. Tian, Q.-D. Chen, H.-B. Sun, Non-Abelian Thouless pumping in photonic waveguides. *Nat. Phys.* **18**, 1080–1085 (2022).
34. B.-Y. Xie, O. You, S. Zhang, Photonic topological pump between chiral disclination states. *Phys. Rev. A* **106**, L021502 (2022).
35. S. Longhi, Topological pumping of edge states via adiabatic passage. *Phys. Rev. B* **99**, 155150 (2019).
36. J.-L. Tambasco, G. Corrielli, R. J. Chapman, A. Crespi, O. Zilberberg, R. Osellame, A. Peruzzo, Quantum interference of topological states of light. *Sci. Adv.* **4**, aat3187 (2018).
37. S. Hu, Y. Ke, C. Lee, Topological quantum transport and spatial entanglement distribution via a disordered bulk channel. *Phys. Rev. A* **101**, 052323 (2020).
38. Y. Wang, Y.-H. Lu, J. Gao, K. Sun, Z.-Q. Jiao, H. Tang, X.-M. Jin, Quantum topological boundary states in quasi-crystals. *Adv. Mater.* **31**, e1905624 (2019).
39. M. Born, V. Fock, Beweis des Adiabatensatzes. *Zeitschrift für Physik* **51**, 165–180 (1928).
40. L. I. Schiff, *Quantum Mechanics* (McGraw-Hill, 1981).
41. D. Comparat, General conditions for quantum adiabatic evolution. *Phys. Rev. A* **80**, 012106 (2009).
42. S. Martínez-Garaot, A. Ruschhaupt, J. Gillet, T. Busch, J. G. Muga, Fast quasiadiabatic dynamics. *Phys. Rev. A* **92**, 043406 (2015).
43. J. Provost, G. Vallee, Riemannian structure on manifolds of quantum states. *Commun. Math. Phys.* **76**, 289–301 (1980).
44. A. Srivastava, A. Imamoglu, Signatures of Bloch-band geometry on excitons: Nonhydrogenic spectra in transition-metal dichalcogenides. *Phys. Rev. Lett.* **115**, 166802 (2015).
45. O. Bleu, G. Malpuech, Y. Gao, D. D. Solnyshkov, Effective theory of nonadiabatic quantum evolution based on the quantum geometric tensor. *Phys. Rev. Lett.* **121**, 020401 (2018).
46. S. Peotta, P. Törmä, Superfluidity in topologically nontrivial flat bands. *Nat. Commun.* **6**, 8944 (2015).
47. X. Tan, D.-W. Zhang, Z. Yang, J. Chu, Y.-Q. Zhu, D. Li, X. Yang, S. Song, Z. Han, Z. Li, Y. Dong, H.-F. Yu, H. Yan, S.-L. Zhu, Y. Yu, Experimental measurement of the quantum metric tensor and related topological phase transition with a superconducting qubit. *Phys. Rev. Lett.* **122**, 210401 (2019).
48. A. Gianfrate, O. Bleu, L. Dominici, V. Ardizzone, M. De Giorgi, D. Ballarini, G. Lerario, K. W. West, L. N. Pfeiffer, D. D. Solnyshkov, D. Sanvitto, G. Malpuech, Measurement of the quantum geometric tensor and of the anomalous Hall drift. *Nature* **578**, 381–385 (2020).
49. A. Gao, Y.-F. Liu, J.-X. Qiu, B. Ghosh, T. V. Trevisan, Y. Onishi, C. Hu, T. Qian, H.-J. Tien, S.-W. Chen, M. Huang, D. Bérubé, H. Li, C. Tzschaschel, T. Dinh, Z. Sun, S.-C. Ho, S.-W. Lien, B. Singh, K. Watanabe, T. Taniguchi, D. C. Bell, H. Lin, T.-R. Chang, C. R. Du, A. Bansil, L. Fu, N. Ni, P. P. Orth, Q. Ma, S.-Y. Xu, Quantum metric nonlinear Hall effect in a topological antiferromagnetic heterostructure. *Science* **381**, 181–186 (2023).
50. M. Yu, P. Yang, M. Gong, Q. Cao, Q. Lu, H. Liu, S. Zhang, M. B. Plenio, F. Jelezko, T. Ozawa, N. Goldman, J. Cai, Experimental measurement of the quantum geometric tensor using coupled qubits in diamond. *Natl. Sci. Rev.* **7**, 254–260 (2019).
51. J.-W. Rhim, K. Kim, B.-J. Yang, Quantum distance and anomalous Landau levels of flat bands. *Nature* **584**, 59–63 (2020).
52. M. J. Rice, E. J. Mele, Elementary excitations of a linearly conjugated diatomic polymer. *Phys. Rev. Lett.* **49**, 1455–1459 (1982).
53. D. Vanderbilt, R. D. King-Smith, Electric polarization as a bulk quantity and its relation to surface charge. *Phys. Rev. B* **48**, 4442–4455 (1993).
54. J. K. Asbóth, L. Oroszlány, A. P. Pályi, *A Short Course on Topological Insulators: Band Structure and Edge States in One and Two Dimensions*, vol. 919 of *Lecture Notes in Physics* (Springer International Publishing, 2016).
55. M. Hafezi, S. Mittal, J. Fan, A. Migdall, J. M. Taylor, Imaging topological edge states in silicon photonics. *Nat. Photonics* **7**, 1001–1005 (2013).
56. A. Blanco-Redondo, B. Bell, D. Oren, B. J. Eggleton, M. Segev, Topological protection of biphoton states. *Science* **362**, 568–571 (2018).
57. W. Song, W. Sun, C. Chen, Q. Song, S. Xiao, S. Zhu, T. Li, Breakup and recovery of topological zero modes in finite non-Hermitian optical lattices. *Phys. Rev. Lett.* **123**, 165701 (2019).
58. M. I. Shalaev, W. Walasik, A. Tsukernik, Y. Xu, N. M. Litchinitser, Robust topologically protected transport in photonic crystals at telecommunication wavelengths. *Nat. Nanotechnol.* **14**, 31–34 (2019).
59. X.-T. He, E.-T. Liang, J.-J. Yuan, H.-Y. Qiu, X.-D. Chen, F.-L. Zhao, J.-W. Dong, A silicon-on-insulator slab for topological valley transport. *Nat. Commun.* **10**, 872 (2019).
60. H. Zhao, X. Qiao, T. Wu, B. Midya, S. Longhi, L. Feng, Non-Hermitian topological light steering. *Science* **365**, 1163–1166 (2019).
61. A. Vakulenko, S. Kiriushechkina, D. Smirnova, S. Guddala, F. Komissarenko, A. Alù, M. Allen, J. Allen, A. B. Khanikaev, Adiabatic topological photonic interfaces. *Nat. Commun.* **14**, 4629 (2023).
62. D. Smirnova, S. Kruk, D. Leykam, E. Melik-Gaykazyan, D.-Y. Choi, Y. Kivshar, Third-harmonic generation in photonic topological metasurfaces. *Phys. Rev. Lett.* **123**, 103901 (2019).
63. Y. Xu, L. Li, H. Jeong, S. Kim, I. Kim, J. Rho, Y. Liu, Subwavelength control of light transport at the exceptional point by non-Hermitian metagratings. *Sci. Adv.* **9**, eadf3510 (2023).
64. S. Xia, D. Kaltsas, D. Song, I. Komis, J. Xu, A. Szameit, H. Buljan, K. G. Makris, Z. Chen, Nonlinear tuning of PT symmetry and non-Hermitian topological states. *Science* **372**, 72–76 (2021).
65. M. Mrejen, H. Suchowski, T. Hatakeyama, C. Wu, L. Feng, K. O'Brien, Y. Wang, X. Zhang, Adiabatic elimination-based coupling control in densely packed subwavelength waveguides. *Nat. Commun.* **6**, 7565 (2015).
66. L. C. Venuti, P. Zanardi, Quantum critical scaling of the geometric tensors. *Phys. Rev. Lett.* **99**, 095701 (2007).
67. L.-S. Lin, H.-L. Zhang, Z.-B. Yang, Method for the quantum metric tensor measurement in a continuous variable system. *Photonics* **10**, 256 (2023).
68. S. Longhi, Quantum-optical analogies using photonic structures. *Laser Photon. Rev.* **3**, 243–261 (2009).

Acknowledgments

Funding: We acknowledge the financial support from the National Key R&D Program of China (2022YFA1404301 and 2023YFA1407700), the National Natural Science Foundation of China (nos. 12174186, 12204233, 62288101, 92250304, and 62325504), the New Cornerstone Science Foundation, and the Hong Kong Research Grant Council (AoE/P-701/20, 17309021). T.L. thanks the support from Dengfeng Project B of Nanjing University. **Author contributions:** Conceptualization: W.S. and O.Y. Methodology: W.S., O.Y., J.S., and C.H. Investigation: W.S., O.Y., J.S., S.W., C.C., C.H., and K.Q. Visualization: W.S. and O.Y. Supervision: S.Zhu, S.Zha., and T.L. Writing—original draft: W.S. and O.Y. Writing—review and editing: W.S., O.Y., S.Zha., and T.L. **Competing interests:** The authors declare that they have no competing interests. **Data and materials availability:** All data needed to evaluate the conclusions in the paper are present in the paper and/or the Supplementary Materials.

Submitted 13 December 2023
Accepted 21 June 2024
Published 26 July 2024
10.1126/sciadv.adn5028